Fluorescence resonance energy transfer in near-infrared fluorescent oligonucleotide probes for detecting protein–DNA interactions

Surong Zhang*, Valeri Metelev*†, David Tabatadze‡, Paul C. Zamecnik‡, and Alexei Bogdanov, Jr.*§¶

*Laboratory of Molecular Imaging Probes, Department of Radiology, §Department of Cell Biology, University of Massachusetts Medical School, 55 Lake Avenue North, Worcester, MA 01655; ‡Cancer Center, Massachusetts General Hospital, 149 Thirteenth Street, Charlestown, MA 02129; and †Department of Chemistry, Moscow State University, Moscow 119991, Russian Federation

Contributed by Paul C. Zamecnik, January 23, 2008 (sent for review October 16, 2007)

Optical imaging in the near-infrared (NIR) range enables detecting ligand-receptor interactions and enzymatic activity *in vivo* due to lower scattering and absorption of NIR photons in the tissue. We designed and tested prototype NIR fluorescent oligodeoxyribonucleotide (ODN) reporters that can sense transcription factor NF-κB p50 protein binding. The reporter duplexes included donor NIR Cy5.5 indodicarbocyanine fluorochrome linked to the 3′ end of the first ODN and NIR acceptor fluorochromes (indodicarbocyanine Cy7 or, alternatively, a heptamethine cyanine IRDye 800CW) that were linked at the positions +8 and +12 to the complementary ODN that encoded p50 binding sites. Both Cy7 and 800CW fluorochromes were linked by using hydrophilic internucleoside phosphate linkers that enable interaction between the donor and the acceptor with no base-pairing interference. We observed efficient fluorescence resonance energy transfer (FRET) both in the case of Cy5.5–Cy7 and Cy5.5–800CW pairs of fluorochromes, which was sensitive to the relative position of the dyes. Higher FRET efficiency observed in the case of Cy5.5–Cy7 pair was due to a larger overlap between the ODN-linked Cy5.5 emission and Cy7 excitation spectra. Fluorescent mobility shift assay showed that the addition of human recombinant p50 to ODN duplexes resulted in p50 binding and measurable increase of Cy5.5 emission. In addition, p50 binding provided a concomitant protection of FRET effect from exonuclease-mediated hydrolysis. We conclude that NIR FRET effect can be potentially used for detecting protein–DNA interactions and that the feasibility of detection depends on FRET efficacy and relative fluorochrome positions within ODN binding sites.

carbocyanine | transcription factor

The ability to image specific DNA–protein interactions directly in intact living systems would greatly expand our ability to directly characterize disease-specific transcriptional activation and downstream signal transduction events *in vivo*. The approaches that use either (*i*) pure proteins and DNA (or RNA) binding probes or (*ii*) genetic reporter constructs positioned under the control of specific transcription-factor binding elements are routinely used in transcription factor research. The former are classic methods based on changes in fluorescence spectra, spectral anisotropy and fluorescence lifetimes that either rely on protein tryptophans as "endogenous probes" (1–3), or use protein and ODN probe labeling with fluorochromes (4–7). These methods require cell homogenization and isolation of nucleic-acid binding proteins, usually as crude "nuclear extract" and are not compatible with *in vivo* research. The latter (i.e., genetic reporters) are suitable for *in vivo* research because cells bearing genetically encoded reporters can be selected, expanded and transferred *in vivo* with subsequent imaging of regulated gene expression. However, the genetic reporter strategy does not always allow a straightforward comparative analysis of transcription factor activity or transcription factor concentration in various cells. This is primarily a consequence of the fact that the marker gene detection/imaging technology depends on the signal produced by the marker protein product of gene expression rather than the active transcription factor. This introduces "uncertainty factors" involving marker gene mRNA stability as well as proteolysis that may proceed at variable rates in various cells. For example, in recent investigation of TNF-α mediated NF-κB activation, a 3-h delay between NF-κB activation and marker gene expression, translation, and protein folding was detected. This finding suggested a significant "disconnect" between transcriptional activation and the "imageable" signal production (8). Therefore, the analysis of DNA/RNA-binding in live cells with intact genomes would require exogenous imaging probes. For example, direct recognition of proteins can be achieved by using stem-loop aptamers with a fluorochrome/quencher pair attached to the oligonucleotide termini (9, 10). Upon the interaction with a target, the aptamer changes conformation with the release of fluorescence. Alternatively, fluorescent protein-binding duplex probes based on the effect of ODN duplex protection from degradation by exonucleases could potentially be used (11). The above SYBR-labeled probes show high fluorescence only in the intact state (i.e., protected from the degradation by DNA-bound protein). Finally, efficient fluorescence dequenching was observed upon *E.coli* single-stranded DNA binding protein interaction with a hairpin-like beacon (12). The caveat is in the need for the reporter ODN probes (i.e., beacons and aptamers) to cross plasma membranes and reach the sites of intended action (13). However, the recent finding of an increased cellular tropism of fluorescent ODN duplexes (14) suggests that structural design and optimization of ODN probes could potentially greatly increase their biological activity.

The NF-κB protein family has a pivotal role in transcriptional control of diverse gene families involved in inflammation and cancer (15–17). We previously hypothesized that, because canonical as well as alternative mechanisms of NF-κB activation are critically dependent on the maturation of p50, which unlike most of NF-κB protein family is generated by proteolysis of NF-κB1 p105 precursor (15, 18), the presence of p50, its hetero- or homodimers could be detected by fluorescence sensing and attributed to NF-κB activation. This hypothesis is supported by highly favorable K_D values for Ig-κB box sequence (16–78 pM, depending on the presence of salts (19) and the interaction between DNA-contacting loops and phosphate residues of DNA binding site (20, 21). We previously investigated properties of self-quenched fluorescent NF-κB specific hairpin decoys (22)

Author contributions: A.B. designed research; S.Z. and V.M. performed research; V.M. and D.T. contributed new reagents/analytic tools; S.Z., V.M., P.C.Z., and A.B. analyzed data; and P.C.Z. and A.B. wrote the paper.

The authors declare no conflict of interest.

¶To whom correspondence should be addressed. E-mail: alexei.bogdanov@umassmed.edu.

This article contains supporting information online at www.pnas.org/cgi/content/full/0800162105/DC1.

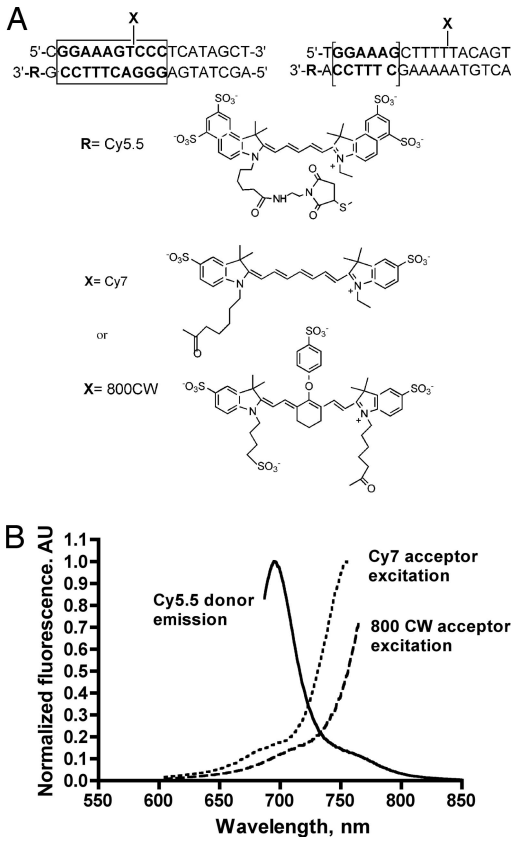

Fig. 1. Probe sequence, fluorochromes and their spectral properties. (*A*) structures of ODN duplex FRET NF-κB probes with the full-length GGAAAGTCCC and truncated GGAAAG binding sites. FRET effect was achieved using Cy5.5 (R) as a donor of fluorescence, and Cy7 or 800CW (X) as acceptors. (*B*) Spectral overlap between Cy5.5 donor emission (solid line) and Cy7 acceptor excitation (dotted line) or 800CW acceptor excitation (dashed line).

bearing fluorochromes on both 3′ and 5′ ends and used them in cell culture experiments as transcription factor decoys (23).

The optimization of decoy-based imaging probes can be potentially achieved by using a simplified two-ODN duplex approach which enables testing combinations of protein binding sites and fluorochromes without the need to purify longer hairpin-forming ODN probes. In this report we: (*i*) investigated new amino-terminated linkers for linking fluorochromes to ODN probes; (*ii*) tested FRET effect between the pair of NIR fluorochromes linked to the complementary strands of duplexes; and (*iii*) tested whether FRET NIR pairs could be used as reporters of NF-κB p50 interaction with specific sequences.

Results

We chose the FRET reporter duplex design that included a pair of near-infrared fluorochromes. The acceptor of fluorescence (Cy7 or 800CW) was linked via an amino group introduced close to the p50 binding sequence whereas the donor fluorochrome (Cy5.5) was linked to the 3′-end of the complementary ODN (Fig. 1*A*). Five ODNs were synthesized, purified and tested for duplex formation [Table 1 and supporting information (SI) Table 2]. These ODNs included: (*i*) ODN1 bearing human β2-microglobulin κB box sequence (5′-GGAAAGTCCC-3′) (24), which was used primarily as a control for (*ii*) ODN2, which had a novel internucleoside phosphate triethylene glycol amino linker positioned after the first thymidine within 5′-GGAAAGTCCC-3′ binding sequence; ODN2 was used to prepare covalent conjugates with Cy7 and 800CW dyes; (*iii*) complementary ODN3 that had a 3′-dithiopropyl linker for conjugating fluorochromes using corresponding maleimides; ODN3 was used to synthesize conjugates with Cy5.5; (*iv*) ODN4 having a truncated NF-κB p50 binding site GGAAAG and internucleoside phosphate triethylene glycol amino linker positioned five bases downstream from the last guanine in the binding site; (*v*) a complementary ODN5 that was similar to ODN3 in that it also had a 3′-dithiopropyl linker. These ODNs were characterized by electrospray mass-spectrometry, which showed a good correlation between the calculated and observed *m/z* values (Table 1). The observed difference in masses between ODN1 and ODN2 pointed to the presence of an internucleoside phosphate-linked $(OCH_2CH_2)_3NH_2$ group. The synthetically introduced linker groups were useful for high-yield linking of fluorochromes to ODNs. By comparing internucleoside phosphate linkers to nucleic acid base-linked amino groups we established that the latter were resulting in fluorochrome-linked products with 2.5-fold lower yields than the former (described in detail in ref. 25).

The FRET between Cy5.5 and the acceptor fluorochrome was observed after Cy5.5-ODN3 was incubated with Cy7- or 800CW-linked to complementary ODN2 (see Fig. 2 *A* and *B*). The decrease of Cy5.5 emission and the increase of the acceptor emission were observed for all pairs of complementary ODNs and donor/acceptor pairs used in our study (Fig. 2). In the presence of internucleoside phosphate-linked Cy7 on the complementary strand we observed more than 10 times lower fluorescence of Cy5.5 measured at 700 nm (λex = 675 nm) and a 3-fold higher fluorescence of Cy7 (if compared with the duplex formed between Cy7-ODN2 and ODN3) (Fig. 2). The formation of duplexes and reversible FRET effects were further studied in more detail by following sigmoidal dependence of the temperature-dependent increase of Cy5.5 fluorescence in a microcuvette of a spectrofluorometer. These experiments enabled measurement of two parameters: melting temperatures and the overall FRET efficacy (SI Table 2).

Table 1. Oligonucleotides and their conjugates used in the study

ODN	Sequence	Mass-spec, *m/z* Calculated	Mass-spec, *m/z* Measured	Modification
ODN1	5′-CGG AAA GTC CCT CAT AGC T-3′	5777.2	5771.6	NA
ODN2	5′-CGG AAA GT*C CCT CAT AGC T-3′	5904.0	5904.2	CW800, Cy7
		6888.9	6888.0 (800CW)	
ODN3	5′-AGC TAT GAG GGA CTT TCC GY-3′	6087.9	6087.6	3′-Cy5.5
		7036.0	7035.9 (Cy5.5)	
ODN4	5′-TGG AAA GCT TTT* TAC AGT T-3′	5964.1	5964.4	CW800, Cy7
		6949.0	6950.0 (800CW)	
ODN5	5′-AAC TGT AAA AAG CTT TCC AY-3′	ND		3′- Cy5.5

T* is T-O-P((OH)=O)-$OCH_2CH_2OCH_2CH_2OCH_2CH_2NH_2$ for native form; Y = $HOCH_2CH_2SSCH_2CH_2CH_2O$-(O=(HO))P-O-; ND, not done; NA, not applicable.

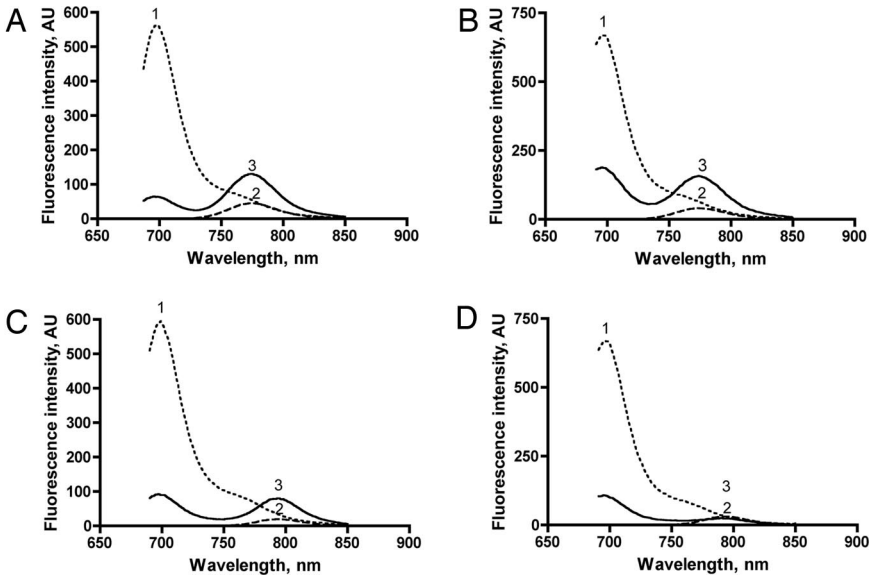

Fig. 2. Fluorescence spectra of ODN duplexes measured using $\lambda = 675$ nm for excitation of Cy5.5 fluorescence. Curve 1 shows fluorescence of the donor, curve 2 shows fluorescence of the acceptor, and curve 3 shows the FRET effect. (*A*) FRET between Cy5.5. (donor) and Cy7 (acceptor) at the distance of 8 nt. Curve 1, ODN3/Cy5.5-ODN3; curve 2, Cy7-ODN2/ODN3; curve 3, Cy7-ODN2/Cy5.5-ODN3. (*B*) FRET between Cy5.5 (donor) and 800 CW (acceptor) at the distance of 8 nt. Curve 1, ODN3/Cy5.5-ODN3; curve 2, 800CW-ODN2/ODN3; curve 3, 800CW-ODN2/Cy5.5-ODN3. (*C*) FRET between Cy5.5. (donor) and Cy7 (acceptor) at the distance of 12 nt. Curve 1, ODN4/Cy5.5-ODN5; curve 2, Cy7-ODN4/ODN5; curve 3, Cy7-ODN4/Cy5.5-ODN5. (*D*) FRET between Cy5.5 (donor) and 800 CW (acceptor) at the distance of 12 nt. Curve 1, ODN4/Cy5.5-ODN5; curve 2, 800CW-ODN4/ODN5; curve 3, 800CW-ODN4/Cy5.5-ODN5.

In general, FRET efficacies were higher in the case of Cy5.5–Cy7 donor–acceptor pair than in the case of Cy5.5–800CW pair, particularly in the case of ODN4/ODN5 duplexes, which showed a 10% lower FRET efficiency if compared with the Cy5.5–Cy7 donor–acceptor pair (SI Table 2). ODN2/ODN3 duplexes (800CW-ODN2/Cy5.5-ODN3 and Cy7-ODN2/Cy5.5-ODN3) gave higher FRET efficacies than the corresponding donor–acceptor pairs in the case of ODN4/ODN5 duplexes (SI Table 2). Fluorescence spectral measurements confirmed this observation (compare Fig. 2 *A* and *B* with *C* and *D*). The higher efficacy of FRET was a consequence of a more extensive overlap between the emission spectrum of Cy5.5 (λex = 675 nm) and the excitation spectrum of Cy7 acceptor than that of 800CW (Fig. 1*B*). The area of spectral overlap in the case of Cy5.5–Cy7 was 26% higher than in the case of Cy5.5–800CW donor–acceptor pairs (Fig. 1*B*).

The measurements of melting temperatures suggested a complete separation of ODNs with temperature increase and, consequently, the loss of FRET effect. Compared with ODN1/ODN3 and ODN2/ODN3 duplexes ODN4/ODN5 duplexes had lower melting temperature due to a higher A-T content (68% vs. 48%). We observed a small temperature shift after the linking of fluorochrome pairs to the duplex-forming ODNs if compared with UV (260 nm) measurements performed using nonlabeled ODN1-ODN3 duplex (SI Table 2). The measurements of spectral overlaps in Cy5.5–Cy7 and Cy5.5–800CW donor–acceptor pairs and FRET efficacies enabled estimations of the effective distances between the pairs of fluorochromes in different ODN duplexes (see *SI Text*). Cy7–ODN2/Cy5.5–ODN3 duplex [average FRET efficiency (*E*) was 86%] was 49.4 Å; the longest, 64.7 Å, was measured in 800CW-ODN4/Cy5.5-ODN5 duplex (E = 60.7%).

The binding of NF-κB p50 to duplexes was initially followed by using two methods: electrophoretic mobility shift assay (EMSA) in polyacrylamide gels, and fluorescence energy transfer loss measurements after adding p50 to the duplex in solution. In the first case, the components of the mixture are off equilibrium because the free duplex is separated due to a faster migration in electric field during the analysis. The second method afforded measurements at the equilibrium but the observed fluorescence change values are affected by the background fluorescence due to the presence of the free duplex. After resolving the reaction mixture on 10% polyacrylamide gels we observed a typical fluorescence shift to the area close to the origin of electrophoresis, suggesting the formation of a high-molecular mass complex between p50 and the fluorescent duplex. Fluorescence of both free and bound duplex could be imaged by using a transillumination scanner and CCD camera that detected emitted light at two wavelengths: 700 nm (Fig. 3*A*)

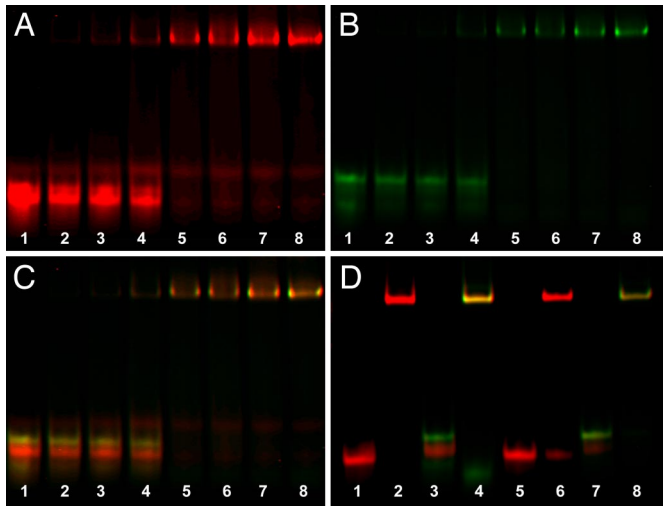

Fig. 3. Two wavelength EMSA. (*A–C*) Concentration dependence of p50 binding to Cy7-ODN2/Cy5.5-ODN3. (*A*) Emission at 700 nm. (*B*) Emission at 800 nm. (*C*) Overlay. In *A–C*, p50 amounts were: lane 1, control, 0 ng; lane 2, 50 ng; lane 3, 100 ng; lane 4, 200 ng; lane 5, 300 ng; lane 6, 400 ng; lane 7, 500 ng; lane 8, 600 ng. (*D*) EMSA of p50 binding to two alternative probe types. Lane 1, 0 ng p50, ODN1/Cy5.5-ODN3; lane 2, 300 ng p50, ODN1/Cy5.5-ODN3; lane 3, 0 ng p50, Cy7-ODN2/Cy5.5-ODN3; lane 4, 300 ng p50, Cy7-ODN2/Cy5.5-ODN3; lane 5, 0 ng p50, ODN4/Cy5.5-ODN5; lane 6, 300 ng p50, ODN4/Cy5.5-ODN5; lane 7, 0 ng p50, Cy7-ODN4/Cy5.5-ODN5; lane 8, 300 ng p50, Cy7-ODN4/Cy5.5-ODN5.

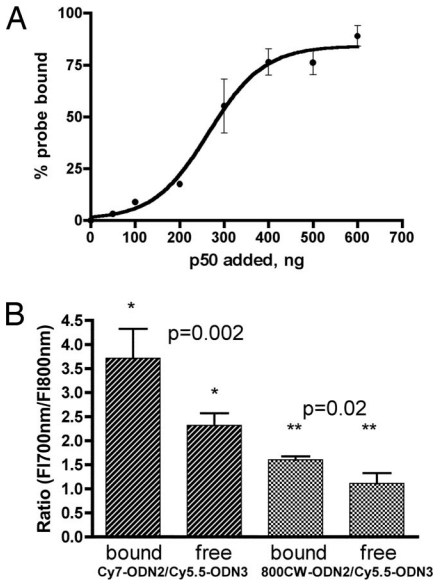

Fig. 4. Quantitative assessment of FRET. (*A*) Quantitation of concentration-dependent EMSA shift of p50 by measuring fluorescence emission at 700 nm: binding to Cy7-ODN2/Cy5.5-ODN3. Results are shown as mean ± SD ($n = 2$, Boltzmann sigmoidal fit, $r^2 = 0.96$). (*B*) Ratiometric measurement of fluorescence intensities (700 nm and 800 nm) using free and p50-bound probes Cy7-ODN2/Cy5.5-ODN3 and 800CW-ODN2/Cy5.5-ODN3. Results are shown as mean ± SD ($n = 3$).

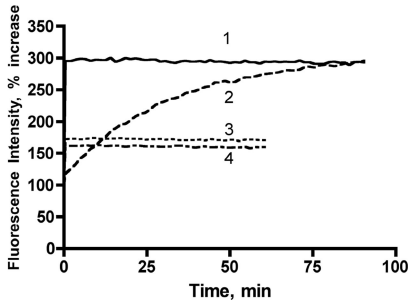

Fig. 5. Effects of exonuclease III (1 unit per sample) mediated hydrolysis on Cy5.5 donor fluorescence changes as measured in the absence (lines 1 and 3) and in the presence (lines 2 and 4) of p50 using Cy7-ODN2/Cy5.5-ODN3 (lines 1 and 2) or Cy7-ODN4/Cy5.5-ODN5 (lines 3 and 4) probes.

and 800 nm (Fig. 3*B*; fused image in Fig. 3*C*). Interestingly, both full-length (duplex 800CW-ODN2/Cy5.5-ODN3) and truncated p50 binding sites (duplex 800CW-ODN4/Cy5.5-ODN5) showed typical migration shifts (Fig. 3*D*). However, by comparing Cy5.5-labled duplexes (ODN2/Cy5.5-ODN3 and ODN4/Cy5.5-ODN5) we determined that in the case of full-length binding sites 94% of probe fluorescence comigrated with p50, whereas 63% comigrated with ODN4/Cy5.5-ODN5 duplex (Fig. 3*D*) at the near-saturating concentrations of recombinant p50 monomer (600 nM).

Recombinant p50 showed a concentration-dependent binding that allowed semiquantitative measurements of donor and acceptor fluorescence intensities (Fig. 4). By measuring fluorescence intensities at various p50 concentrations (10–600 ng, 4–240 nM) and at the constant duplex concentration (1.8 nM Cy7-ODN2/Cy5.5-ODN3 duplex), we determined that binding curves had sigmoidal shape, which suggests a strong cooperativity of p50-probe interaction with duplexes, consistent with the formation of p50 homodimer (p105)–ODN probe complexes (Fig. 4*A*). The half-maximal amount of p50 was 238–300 ng (corresponding to ≈600 nM). The binding to the duplex resulted in a measurable change of Cy5.5 fluorescence in the bound duplex if compared with free duplex. By measuring the ratio of fluorescence intensities at 700 and 800 nm in the shifted band (protein-duplex complex), we determined that in the case of Cy7-ODN2/Cy5.5-ODN3 the ratio (3.7 ± 0.4) was significantly higher than that in the free ODN duplex (2.3 ± 0.2, $P = 0.002$) (Fig. 4*B*). Similar trend was observed if 800CW dye was used as Cy5.5 fluorescence acceptor and the differences were also significant ($P = 0.02$). Although both types of fluorescent duplex probes, i.e., having a full-length NF-κB binding sequence (ODN2/ODN3) and a truncated binding sequence (ODN4/ODN5), showed electrophoretic shifting, we were unable to measure any significant fluorescence changes in EMSA bands in the case of ODN4/ODN5 for both Cy5.5–800CW and Cy5.5–Cy7 donor/acceptor pairs. The above measurements of p50-mediated changes of FRET efficacy were validated by using spectral measurements. Fluorescence was excited using 685 and 785 nm light, emulating a gel infrared imaging system. By comparing ratios of fluorescence intensities measured at 700 and 800 nm, we determined that the total lack of FRET in the presence of Exo III resulted in a 700/800 ratio of 4.5 ± 0.1 in the case of Cy7-ODN2/Cy5.5-ODN3 and 5.6 ± 0.3 in the case of Cy7-ODN4/Cy5.5-ODN5. The baseline FRET ratios in the absence of Exo III were at 1.8 ± 0.4 and 3.6 ± 0.2, respectively, i.e., in the range measured using EMSA gels.

Finally, we investigated whether p50 protected donor–acceptor interaction from the degradation by exonuclease (Fig. 5). The addition of the 250-times molar excess of p50 protein (calculated as homodimer) to the solution of Cy7-ODN2/Cy5.5-ODN3 resulted in a measurable, small but overall significant increase of Cy5.5 fluorescence (106–109% increase at λex = 675/λem = 696 nm). The addition of 1 unit of Exo III to this solution resulted in a gradual increase of fluorescence at 696 nm, i.e., the half-maximum of fluorescence was reached at $t_{1/2} = 22.5$ min. In contrast, in the absence of p50 protein the increase of Cy5.5 fluorescence was almost instantaneous (Fig. 5, solid line). The protection of Cy7-ODN3/Cy5.5-ODN4 by p50 was much less efficient because, both in the presence and absence of p50, Exo III-mediated degradation of the duplex showed almost no detectible differences in kinetics (Fig. 5).

Discussion

FRET was originally proposed by us as a tool for investigating interactions between complementary ODNs (4). More recently, FRET found multiple applications as a method of choice for designing oligonucleotide-based molecular beacon assays (26, 27). Molecular beacon technology was subsequently married with nanotechnology, leading to a development of gold nanoparticle probes linked to fluorescent antisense oligonuclotides (28, 29). Our research had a goal of extending the use of ODN FRET probe for sensing interactions between specific binding sites within double-stranded DNA sequences and proteins. Our approach is based on the observation of an emission–excitation spectral overlap between the pairs of near-infrared fluorochromes, which are superior to other fluorochromes for *in vivo* optical imaging due to the markedly lower near-infrared fluorescent light scattering and absorption in the tissue (30–32). In our experiments, we chose a commonly used near-infrared fluorochrome Cy5.5, which can be excited using widely available laser diodes (33, 34) and used it as a donor of emitted photons. Near infrared Cy7 and 800CW fluorochromes with farther red-shifted excitation spectra served as acceptors of Cy5.5 emission. The fluorescence of Cy5.5 donor was excited at a wavelength corresponding to a low molar absorbance of the acceptors minimizing the direct excitation of the acceptor and increasing the fraction of acceptor fluorochrome available for energy transfer. We anticipated that near-infrared FRET could potentially enable

ratiometric measurements of fluorescence changes in two channels (at 700 and 800 nm), both of which are suitable for imaging in live animals. We further used the observed FRET effect for detecting the degree of juxtaposition of the fluorochrome pair within ODN duplexes. Such duplexes provided a molecularly constrained environment that facilitated resonance energy transfer. Moreover, we hypothesized that by encoding p50 NF-κB transcription factor binding sequences in the ODN duplex we should be able to detect transcription factor-ODN duplex binding by measuring changes in near-infrared FRET efficacy. Such change would be a result of a distance change between the dye pairs or other potential interference with FRET as a result of protein binding through multiple contacts of protein DNA binding loops with the ODN (20, 21). To test this assumption, we covalently linked fluorescence donor (Cy5.5) via 3′ end of ODN and conjugated the acceptor to the complementary ODN through a hydrophilic linker at the internucleoside phosphate position. The above strategy allowed us to achieve high ODN modification yields with fluorescent dyes, minimize interference with base pairing, and afford potential screening of various positions of the dye pair along the sequence for probe optimization using automated ODN synthesis.

In our initial experiments we used two markedly different designs of ODN duplex probes: the first contained 10 bp long binding sequence with short 8-bp distance between the donor and the acceptor. The internucleoside phosphate linker (Fig. 1) was positioned downstream of the phosphodiester bonds that establish multiple hydrogen bonds and hydrophobic contacts with lysine (K144, K145, K241), cysteine (C59) and tyrosine (Y57) of p50 protein (20). The other ODN duplex probe had a 6-bp truncated binding site with a significantly longer 11-bp gap in between the donor/acceptor pair of fluorochromes, both of which were flanking the binding sequence. Interestingly, in both cases we were able to measure FRET between Cy5.5/Cy7 and Cy5.5/800CW pairs. The estimation of Förster distances between the donor and the acceptor in duplexes based on spectral overlap of free fluorochromes in solution suggested that, in general, due to a relatively modest area of spectral overlap, the distance between the donor and acceptor should not exceed 50 Å to achieve high efficacy of FRET. Furthermore, by adding human recombinant p50 NF-κB to the probes and by using shift assay (EMSA), we proved that both ODN duplexes were suitable as probes for detecting ODN binding. The ratiometric measurements performed in EMSA gels showed that donor/acceptor ratios in protein-bound shifted bands were significantly higher than the ratios measured in free ODN duplex bands. However, these differences were measurable only in the case of full-length binding sites encoded by the duplex formed by ODN2 and ODN3 (Fig. 4). The ratiometric measurements of FRET changes benefited from the fact that the binding of p50 protein to the probe resulted in the apparent decrease of FRET efficacy. Because of resonance energy transfer, the loss of the fluorescence of the donor (at 700 nm) was increasing but the acceptor fluorescence (at 800 nm) was decreasing, and the ratiometric measurements resulted in the amplification of the effect of energy transfer loss. Consequently, similar measurements performed using ODN duplex probes with the 5-bp-longer distance between the donor/acceptor pair (ODN4/ODN5) revealed a lack of FRET efficacy decrease. Apparently, the lack of measurable changes in FRET efficacy in the case of truncated binding site probes was due to the longer distance between the donor/acceptor pair combined with the diminished kinetic stability of p50 duplex interaction. The diminished stability was suggested by the measurements done by using exonuclease protection assay (Fig. 5).

Therefore, our results suggest that FRET between a pair of near-infrared dyes is sensitive to protein binding to ODN duplex-encoded sequence and can be potentially used for detecting protein–DNA interactions directly. With further optimization of donor and acceptor fluorochromes and their respective positions along the base pairs that constitute the binding site, one would be able to monitor cognate interactions between transcription factors and specific double-stranded DNA duplex or hairpin-like probes in live cells and, ultimately, in living systems.

Materials and Methods

Oligodeoxyribonucleotide (ODN) Synthesis and Modification. The detailed procedures are described in *SI Text*. ODN2 and ODN4 were synthesized by using a thymidine phosphoramidite synthon (5′-*O*-DMTr-thymidine-3′-*O*-(2-(2-(2-trifluoroacetamidoethoxy)ethoxy)ethyl)-*N*,*N*-diisopropylphosphoramidite; ref. 25) with a protected primary amino group linked via a triethylene glycol linker to phosphorus (see SI Fig. 6).

Spectral Measurements. All UV spectral measurements were performed at room temperature unless otherwise noted using Cary 50 spectrophotometer (Varian). All fluorescence measurements were carried out at room temperature unless otherwise noted in quartz microcuvettes using a Cary Eclipse Fluorescence Spectrophotometer (Varian). Melting temperatures were determined with a stepwise Peltier temperature ramping bath in 2° mode in a temperature-controlled cuvette holder. To measure p50 binding or p50-mediated protection against exonuclease degradation, 43 fmol of fluorescent duplex (final concentration, 0.54 nM) were added to the protein binding buffer (10 mM Tris, 100 mM KCl, 2 mM $MgCl_2$, 0.1 mM EDTA, 0.1 mg/ml yeast tRNA, 10% vol/vol glycerol, 0.25 mM DTT, pH 7.5), and spectral measurements were taken at room temperature as above. Human recombinant p50 protein (Alexis Biochemicals or Active Motif) in 4.3 μl at 300 ng/μl (final concentration, 0.3 μM) were added and fluorescence measurements were performed immediately, and then every 1.5 min for 30 min. In control experiments, human serum albumin (HSA, essentially fatty acid-free; Sigma) or protein binding buffer were used as controls. After the above spectral measurements were taken, exonuclease III (Exo III, 1 unit; Promega) was added and the mixture was subjected to fluorescence measurement immediately every 1.5 min for 1 h. To validate measurements performed using Odyssey infrared imaging system (see below), we used excited fluorescence of Cy7/Cy5.5 and 800CW/Cy5.5 labeled duplexes at 685 and 785 nm and collected fluorescence emitted at 700 and 800 nm. To eliminate FRET effect we added Exo III as described above and repeated the measurements. The fluorescence intensity ratios measured at 700 and 800 nm were compared with the ratios derived from the measurements obtained using Odyssey system.

Preparation of ODN Duplexes. ODN duplexes were prepared by mixing the ODNs in a 1:1 molar ratio unless otherwise noted, in buffer solution containing 25 mM Hepes, 1 mM $MgCl_2$, and 50 mM NaCl. The duplex mixtures were heated between 90–95°C, 5 min to dissociate any intrastrand duplexes, and allowed to cool at room temperature to attain equilibrium.

EMSAs. EMSAs were performed using a reaction mixture containing the fluorochrome-labeled double-stranded ODN duplexes (final concentration, 1.8 nM), 50–600 ng of human recombinant p50 (final concentration, 0.1–1.2 μM; Alexis Biochemicals) or HeLa nuclear extract (5 μg, Promega) that was incubated for 30 min at room temperature in a volume of 10 μl in the presence of protein binding buffer (10 mM Tris, 100 mM KCl, 2 mM $MgCl_2$, 0.1 mM EDTA, 0.1 mg/ml tRNA, 10% glycerol, 0.25 mM DTT, pH 7.5). Samples were loaded and run on 10% TBE Gels (Bio-Rad) in 0.5×TBE buffer. Imaging and digitizing was performed on Odyssey Infrared Imaging system (Li-Cor). Fluorescence of bound and free bands was determined by using simultaneous solid diode excitation at 685 and 785 nm and measured using a dichroic mirror transmitting above 810 nm (''800 nm'' fluorescence band) and reflecting below 750 nm (''700 nm'' fluorescence band). Fluorescence signals were processed to filter scattered and stray light. The obtained images (16 bit TIFF) were analyzed, colorized, and fused using ImageJ 1.38 (NIH).

Statistical Analysis. All experiments were performed in triplicate. Values are expressed as the mean ± the standard deviation (SD) and compared using double-tailed unpaired *t* test with Welch's correction (Prism 4.0, GraphPad).

ACKNOWLEDGMENTS. We thank Mrs. Karen Pierson for technical assistance and Lin He, Doctorate Candidate, School of Mathematical Sciences, Beijing Normal University, Beijing PRC for assistance with the analysis of spectral data. This work was supported in part by grants from The G. Harold and Leila V. Mathers Foundation and National Institutes of Health Grant 5 R01 AI060872–02. S.Z., V.M. and A.B. were supported in part by National Cancer Institute, Exploratory Grant R21 CA116144 (to A.B.).

1. Shore VG, Pardee AB (1956) Energy transfer in conjugated proteins and nucleic acids. *Arch Biochem Biophys* 62:355–368.
2. Bandyopadhyay PK, Wu CW (1978) Fluorescence and chemical studies on the interaction of Escherichia coli DNA-binding protein with single-stranded DNA. *Biochemistry* 17:4078–4085.
3. Bujalowski W, Lohman TM (1989) Negative co-operativity in Escherichia coli single strand binding protein-oligonucleotide interactions. I. Evidence and a quantitative model. *J Mol Biol* 207:249–268.
4. Cardullo RA, Agrawal S, Flores C, Zamecnik PC, Wolf DE (1988) Detection of nucleic acid hybridization by nonradiative fluorescence resonance energy transfer. *Proc Natl Acad Sci USA* 85:8790–8794.
5. Perez-Howard GM, Weil PA, Beechem JM (1995) Yeast TATA binding protein interaction with DNA: Fluorescence determination of oligomeric state, equilibrium binding, on-rate, and dissociation kinetics. *Biochemistry* 34:8005–8017.
6. Delahunty MD, Wilson SH, Karpel RL (1994) Studies on primer binding of HIV-1 reverse transcriptase using a fluorescent probe. *J Mol Biol* 236:469–479.
7. Bailey M, *et al.* (1995) Interaction between the Escherichia coli regulatory protein TyrR and DNA: A fluorescence footprinting study. *Biochemistry* 34:15802–15812.
8. Hellweg C, Baumstark-Khan C, Horneck G (2003) Generation of stably transfected mammalian cell lines as fluorescent screening assay for NF-kappa B activation-dependent gene expression. *J Biomol Screening* 8:511–521.
9. Li J, Fang X, Tan W (2002) Molecular aptamer beacons for real-time protein recognition. *Biochem Biophys Res Commun* 292:31–40.
10. Hamaguchi N, Ellington A, Stanton M (2001) Aptamer beacons for the direct detection of proteins. *Anal Biochem* 294:126–131.
11. Chen Z, Ji M, Hou P, Lu Z (2006) Exo-Dye-based assay for rapid, inexpensive, and sensitive detection of DNA-binding proteins. *Biochem Biophys Res Commun* 345:1254–1263.
12. Li JJ, Fang X, Schuster SM, Tan W (2000) Molecular beacons: A novel approach to detect protein-DNA interactions. *Angew Chem Int Ed Engl* 39:1049–1052.
13. Thierry AR, *et al.* (2003) Cellular uptake and intracellular fate of antisense oligonucleotides. *Curr Opin Mol Ther* 5:133–138.
14. Astriab-Fisher A, Fisher MH, Juliano R, Herdewijn P (2004) Increased uptake of antisense oligonucleotides by delivery as double stranded complexes. *Biochem Pharmacol* 68:403–407.
15. Baeuerle PA, Henkel T (1994) Function and activation of NF-kappa B in the immune system. *Annu Rev Immunol* 12:141–179.
16. Baldwin AS (2001) Control of oncogenesis and cancer therapy resistance by the transcription factor NF-kappaB. *J Clin Invest* 107:241–246.
17. Darnell JE, Jr (2002) Transcription factors as targets for cancer therapy. *Nat Rev Cancer* 2:740–749.
18. Baldwin AS, Jr (1996) The NF-kappa B and I kappa B proteins: New discoveries and insights. *Annu Rev Immunol* 14:649–683.
19. Hart DJ, Speight RE, Cooper MA, Sutherland JD, Blackburn JM (1999) The salt dependence of DNA recognition by NF-kappaB p50: A detailed kinetic analysis of the effects on affinity and specificity. *Nucleic Acids Res* 27:1063–1069.
20. Ghosh G, van Duyne G, Ghosh S, Sigler PB (1995) Structure of NF-kappa B p50 homodimer bound to a kappa B site. *Nature* 373:303–310.
21. Muller CW, Rey FA, Sodeoka M, Verdine GL, Harrison SC (1995) Structure of the NF-kappa B p50 homodimer bound to DNA. *Nature* 373:311–317.
22. Metelev V, Weissleder R, Bogdanov A, Jr (2004) Synthesis and properties of fluorescent NF-kappa B-recognizing hairpin oligodeoxyribonucleotide decoys. *Bioconj Chem* 15:1481–1487.
23. Laguillier C, *et al.* (2007) Cell death in NF-kappaB-dependent tumour cell lines as a result of NF-kappaB trapping by linker-modified hairpin decoy oligonucleotide. *FEBS Lett* 581:1143–1150.
24. Gobin SJ, Biesta P, Van den Elsen PJ (2003) Regulation of human beta 2-microglobulin transactivation in hematopoietic cells. *Blood* 101:3058–3064.
25. Tabatadze D, *et al.* (2007) A novel thymidine phosphoramidite synthon for incorporation of internucleoside phosphate linkers during automated oligodeoxynucleotide synthesis. *Nucleosides Nucleotides Nucleic Acids* 27:157–172.
26. Tyagi S, Kramer F (1996) Molecular beacons: Probes that fluoresce upon hybridization. *Nat Biotechnol* 14:303–308.
27. Bratu DP (2006) Molecular beacons: Fluorescent probes for detection of endogenous mRNAs in living cells. *Methods Mol Biol* 319:1–14.
28. Taton TA, Mirkin CA, Letsinger RL (2000) Scanometric DNA array detection with nanoparticle probes. *Science* 289:1757–1760.
29. Rosi NL, *et al.* (2006) Oligonucleotide-modified gold nanoparticles for intracellular gene regulation. *Science* 312:1027–1030.
30. Frangioni JV (2003) In vivo near-infrared fluorescence imaging. *Curr Opin Chem Biol* 7:626–634.
31. Ntziachristos V (2006) Fluorescence molecular imaging. *Annu Rev Biomed Eng* 8:1–33.
32. Weissleder R (2006) Molecular imaging in cancer. *Science* 312:1168–1171.
33. Mujumdar RB, Ernst LA, Mujumdar SR, Lewis CJ, Waggoner AS (1993) Cyanine dye labeling reagents: sulfoindocyanine succinimidyl esters. *Bioconj Chem* 4:105–111.
34. Ballou B, *et al.* (1995) Tumor labeling in vivo using cyanine-conjugated monoclonal antibodies. *Cancer Immunol Immunother* 41:257–263.